EPJ Web of Conferences **6**, 39011 (2010)
DOI:10.1051/epjconf/20100639011

Damage and dissipation mechanisms in the dynamic fracture of brittle materials: Velocity driven transition from nominally brittle to quasi-brittle

J. Scheibert[1 2 3,a], C. Guerra[1 4], D. Dalmas[2], and D. Bonamy[1]

[1] CEA, IRAMIS, SPCSI, Group Complex Systems and Fracture, F-91191 Gif-sur-Yvette, France
[2] Unité Mixte CNRS/Saint-Gobain, Surface du Verre et Interfaces, 39 Quai Lucien Lefranc, 93303 Aubervilliers cedex, France
[3] Physics of Geological Processes, University of Oslo, Oslo, Norway
[4] Facultad de Ingeniería Mecánica y Eléctrica, Universidad Autónoma de Nuevo León, Avenida Universidad, S/N, Ciudad Universitaria, C.P. 66450, San Nicolás de los Garza, NL, Mexico

Abstract. We present the results of recent dynamic fracture experiments [Scheibert *et al.*, Phys. Rev. Lett. **104** (2010) 045501] on polymethylmethacrylate, the archetype of nominally brittle materials, over a wide range of crack velocities. By combining velocity measurements and finite element calculations of the stress intensity factor, we determine the dynamic fracture energy as a function of crack speed. We show that the slope of this curve exhibits a discontinuity at a well-defined critical velocity, below the one associated to the onset of micro-branching instability. This transition is associated with the appearance of conics patterns on the fracture surfaces. In many amorphous materials, these are the signature of damage spreading through the nucleation, growth and coalescence of micro-cracks. We end with a discussion of the relationship between the energetic and fractographic measurements. All these results suggest that dynamic fracture at low velocities in amorphous materials is controlled by the brittle/quasi-brittle transition studied here.

1 Introduction

Driven by both technological needs and the challenges of unresolved fundamental questions, dynamic fracture in brittle materials has been widely investigated over the past century. Since the pionneer work of Griffith [1], Orowan[2] and Irwin[3] a coherent theoretical framework, the Linear Elastic Fracture Mechanics (LEFM) has developed. This theory is based on the fact that – in an elastic medium under tensile loading – the mechanical energy released as fracture occurs is entirely dissipated at the crack tip within a small zone so-called process zone. Defining the fracture energy Γ as the energy needed to create two crack surfaces of a unit area, the crack growth velocity is then selected by the balance between the energy flux and the dissipation rate Γv. This yields [4]:

$$\Gamma \simeq (1 - v/c_R)\, K^2(c)/E, \tag{1}$$

where c_R and E are the Rayleigh wave speed and the Young modulus of the material, respectively, and $K(c)$ is the Stress Intensity Factor (SIF) for a quasi-static crack of length c. K depends only on the applied loading and specimen geometry, and characterizes entirely the stress field in the vicinity of the crack front.

[a] e-mail: julien.scheibert@fys.uio.no

LEFM provides a quantitative description of crack motion that agrees well with observations as long as the crack growth is sufficiently slow [5]. However, comparisons between theory and experiments at high speed yield large discrepancies (see [7,6] for recent reviews). In particular, contrary to what is predicted by LEFM, (i) the maximal crack speeds attained experimentally in amorphous materials are far slower than the limiting speed c_R predicted by Eq. (1) and (ii) fracture surfaces become rough at the optical scale at high velocities (the so-called mirror → mist → hackle transition).

The existence of a micro-branching instability [11,12] at a critical velocity $v_b = 0.4c_R$ may explain *part* of this discrepancy: Beyond v_b, the crack motion stops to be a single crack state to become a multiple crack state that cannot be described by Eq. 1 anymore. And it has been argued [10] that v_b sets the limit beyond which experiments start to depart from theory. The understanding and modelling of the micro-branching instability hence yielded many recent theoretical efforts [13–22]. However, a number of puzzling observations remain at smaller velocities. In particular, even for velocities much lower than v_b, (i) the measured dynamic fracture energy is generally much higher than that at crack initiation [10,23–26] and (ii) fracture surfaces roughen over length scales much larger than the microstructure scale (”mist” patterns) [27], the origin of which remains debated [28–37].

In this paper, we present recent results [38] of dynamic fracture experiments in polymethylmethacrylate (PMMA), the archetype of brittle amorphous materials, designed to unravel the primary cause of these last discrepancies. We show that the slope of the dynamic fracture energy as a function of crack speed exhibits a discontinuity at a well-defined critical velocity v_a well below v_b. This transition coincides with the onset of damage spreading through the nucleation, growth and coalescence of micro-cracks, the signature of which is the presence of conic patterns on post-mortem fracture surfaces. We provide a simple interpretation for this nominally brittle to quasi-brittle transition allowing to relate both the energetic and fractographic measurements.

2 Experiments

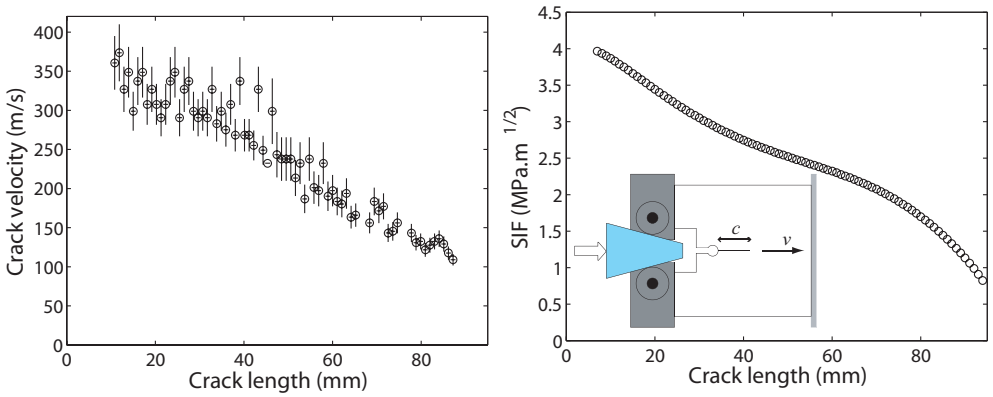

Fig. 1. Adapted from [38]. Left: Measured crack velocity v as a function of crack length c in a typical experiment (U_0=2.6 J). The vertical lines are error bars. Right: Calculated quasi-static SIF K as a function of c. Inset: Schematics of the Wedge-Splitting test.

Dynamic cracks are driven in PMMA with measured Young modulus and Poisson ratio of E=2.8±0.2 GPa and ν=0.36, which yields c_R=880± 30 m.s^{-1}. Its fracture energy at the onset of crack propagation was determined to be K_c^2/E=0.42±0.07 kJ.m^{-2}, with K_c being the material toughness. Fracture tests are performed in a so-called wedge splitting geometry [39]. Parallelipedic specimen of size $140 \times 125 \times 15$ mm^3 in the x (propagation), y (loading) and z (sample thickness) are prepared by cutting out of one of the two 125×15 mm^2 faces a 25×25 square mouth ended by a 10 mm groove.

Two steel jaws equipped with rollers are then placed on both sides of the mouth and a steel wedge (semi-angle 15°) is pushed in between at constant velocity (38 μm/s) up to crack initiation. The SIF K is observed to decrease with the crack length c [40]. In order to increase its value at crack initiation, and therefore the initial crack velocity, a circular hole with a radius ranging between 2 and 8mm is drilled at the tip of the groove to tune the stored mechanical energy U_0, and therefore the range of $K(t)$ and $v(t)$ scanned over a given experiment. Dynamic crack growth with instantaneous velocities ranging from 75 m.s^{-1} to 500 m.s^{-1} and stable trajectories are obtained. The location $c(t)$ of the crack front is measured during each experiment (40 μm and 0.1 μs accuracies) using a modified version of the potential drop technique: A series of 90 parallel conductive lines (2.4 nm-thick Cr layer covered with 23 nm-thick Au layer), 500 μm-wide with an x-period of 1mm are deposited on one of the x-y surfaces of the specimen, connected in parallel and alimented with a voltage source. As the crack propagates, it cuts the conductive lines at successive times that can be detected via an oscilloscope. The instantaneous crack velocity $v(c)$ is computed from $c(t)$. The value of the stress intensity factor $K(c)$ is calculated using 2D finite element calculations (software Castem 2007) on the exact experimental geometry, assuming plane stress conditions and a constant wedge position as boundary condition. The calculations have been checked by comparison with the results of a previous finite elements study by Karihaloo and Xiao [40].

3 Results

3.1 Determination of the fracture energy

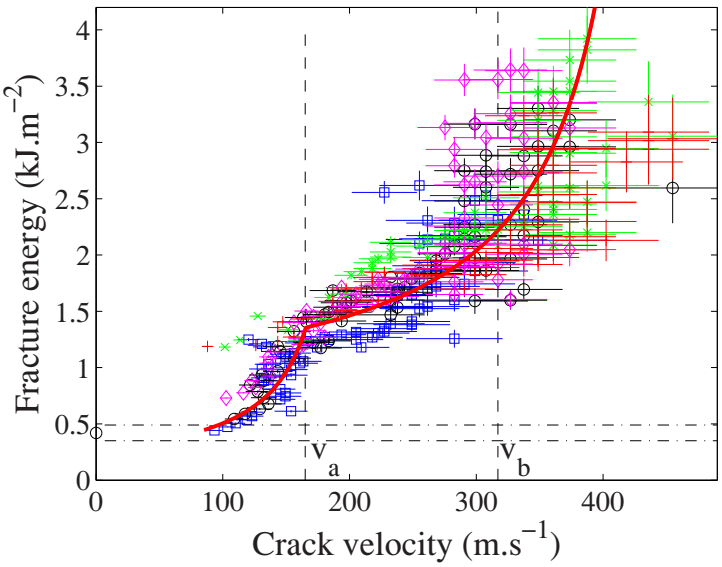

Fig. 2. Adapted from [38]. Fracture energy Γ as a function of crack velocity v for five different experiments with different stored mechanical energies U_0 at crack initiation: 2.0 (□), 2.6 (○), 2.9 (◊), 3.8 (+) and 4.2 J (×). The two vertical dashed lines correspond to v_a and v_b. The two horizontal dashed lines indicate the confidence interval for the measured fracture energy K_c^2/E at crack initiation. Thick line: model prediction (see section 4).

The typical variations of both the crack velocity v and the stress intensity factor K as a function of the crack length c are shown in Fig. 1. From these curves, one can derive the fracture energy Γ using

Eq. 1. Its variations as a function of v, plotted in Fig. 2, is found to be the same in various experiments performed with various stored mechanical energy U_0 >2.0 J at crack initiation. Three regimes can be evidenced on this curve. For slow crack velocities, Γ remains of the order of K_c^2/E as expected in LEFM. Then, as v reaches the first critical velocity $v_a \simeq 165$ m.s^{-1}=0.19 c_R, Γ increases abruptly to a value about 3 times larger than K_c^2/E. Beyond v_a, Γ increases slowly with v up to the second critical velocity, v_b=0.36c_R $\simeq$ 317 m.s^{-1} [10], above which Γ diverges again with v. This second increase corresponds to the onset of the micro-branching instability, widely discussed in the literature [11] [10], whereas the first one, at v_a, was reported in [38] for the first time. The high slope of $\Gamma(v)$ around v_a provides a direct interpretation for the repeated observation of cracks that span a large range of Γ but propagate at a nearly constant velocity of about 0.2c_R (see e.g. refs. [45] [46]).

3.2 Morphology of post-mortem fracture surfaces

To shed light on the nature of the transition at $v = v_a$ evidenced on the curve relating Γ to v (Fig. 2), we examine now the post mortem fracture surfaces. Figure 3 shows the evolution of the surfaces morpholoy as the velocity increases. For v smaller than v_a, the fracture surface remains smooth at the optical scale, as in Fig. 3a (bottom). But above this threshold, conic marks can be evidenced on the fracture surfaces (Figs. 3b and c, bottom). They do not leave any visible print on the side of the specimens (Fig. 3a and b, top), contrary to the micro-branches that start to develop at higher velocities, for $v \geq v_b$ (Fig. 3c, top).

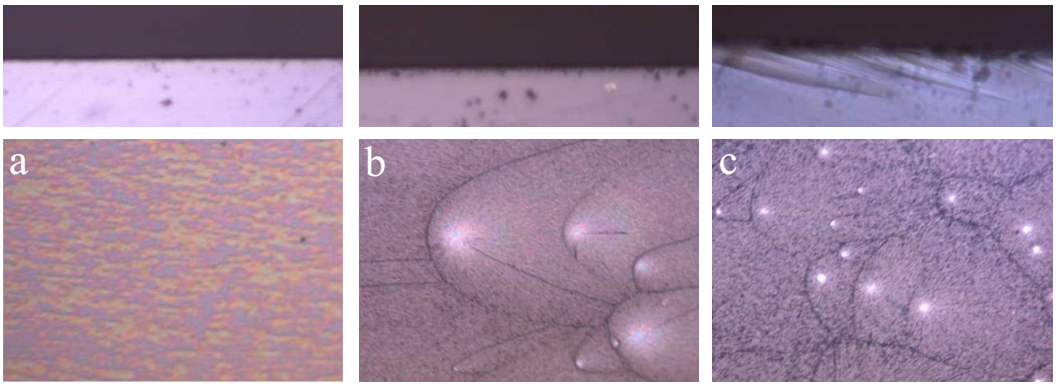

Fig. 3. Adapted from [38]. Microscope images (×10) taken at (a) v=120±20 m.s^{-1}, K^2/E=1 kJ.m^{-2} (b) v=260±30 m.s^{-1}, K^2/E=2 kJ.m^{-2} (c) v=650±100 m.s^{-1} (K^2/E=7 kJ.m^{-2}). Top line : sample sides (0.25 × 0.7 mm^2 field of view). Bottom line : fracture surfaces (0.5 × 0.7 mm^2 field of view). Crack propagation is from left to right.

Similar conic marks were reported in the fracture of other brittle materials, among which polystyrene [41], silicate glasses [42], cellulose acetate [43], polycrystalline materials [44], and Homalite [46]. Their formation is thought [42] to find their origin in the heterogeneous nature of the material, which contains inherent toughness fluctuations at the microstructure scale. The enhanced stress field in the vicinity of the main crack front activates some of the low toughness zones and triggers the initiation of secondary penny-shape microcracks ahead of the crack front. These microcracks grow radially under the stress imposed by the main crack along a plane different from that of the main crack. And when these two fronts intersect in space and time, the ligament separating the two cracks breaks up leaving a conic marking on the post-mortem fracture surface.

Figure 4 shows the surface density of conic marks ρ as a function of crack velocity v. Below v_a, we checked that no conic mark is observable up to ×50 magnification. Above v_a, ρ increases almost linearly with $v - v_a$. The precise correspondence between the critical velocity v_a at which the slope of $\Gamma(v)$ is discontinuous and the velocity at which the first conic marks appear on the fracture surfaces

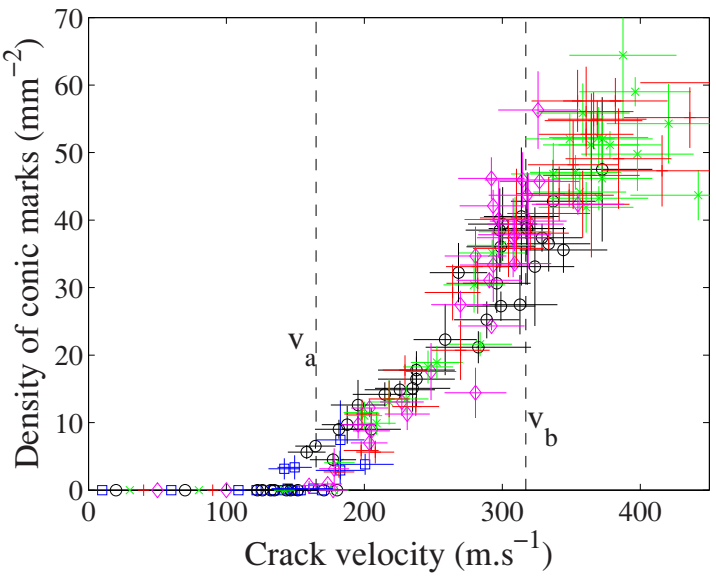

Fig. 4. Adapted from [38]. Surface density ρ of conic marks as a function of crack velocity for the same experiments as in Fig. 2.

strongly suggests that both phenomena are associated with the same transition. The nucleation, growth and coalescence of micro-cracks can therefore be identified as the new fracture mechanism starting at v_a. This damage process is generic in brittle materials and is relevant for an even wider range of materials than those that exhibit conic marks, e.g. granite [47].

4 Interpretation

We turn now to the interpretation of the curves $\Gamma(v)$ between 0 and v_b. In this respect, it is interesting to plot $\Gamma(v)$ as a function of the dynamic SIF $K_d(v)$ (Fig. 5(a)). This quantity can be related to the static SIF K through: $K_d(v) = k(v)K$ [4] where $k(v) \simeq (1 - v/c_R)/\sqrt{1 - v/c_D}$ is universal and c_D is the dilatational wave speed (here c_D=2010±60 m.s^{-1}). Below and above v_a, Γ is found to vary linearly with $K_d(v)^2$ (Note that Γ has been plotted as a function of $K_d(v)^2/E$ rather than $K_d(v)^2$ so that both coordinates are in J/m^2). This scaling is to compare to that of the size $R_c(v)$ of the Fracture Process Zone (FPZ), i.e. the zone where linear elasticity fails and all the dissipative phenomena occur: $R_c(v) = K_d^2(v)/a\sigma_Y^2$ where σ_Y is the yield stress and a is a dimensionless constant (see e.g. [37]).

Let us first look at the regime before micro-cracking ($v \leq v_a$). The affine relation between Γ and $R_c(v)$ suggests that the volume energy ϵ dissipated within the FPZ is constant. Indeed, the volume scanned by the FPZ when the crack surface increases by S is $R_c(v)S$. The dissipated energy $\Gamma(v)S$ is given by $\gamma S + \epsilon R_c(v)S$ where γ is the Griffith surface energy. Since $\Gamma(v = 0) = K_c^2/E$, one finally gets for $v \leq v_a$:

$$\Gamma(v) = \alpha \frac{K_d(v)^2}{E} + (1 - \alpha)\frac{K_c^2}{E} \quad \text{with} \quad \alpha = \frac{2\epsilon E}{a\sigma_Y^2} \tag{2}$$

A linear fit to the data (R=0.985) gives $\alpha = 1.17 \pm 0.05$ and $K_c^2/E = 0.3 \pm 0.2$ kJ.m^{-2} (see Fig. 5(a)). The latter value is compatible with the measurements of the fracture energy at crack initiation.

By combining Eqs. (1) and (2), one gets a prediction for the $\Gamma(v)$ curve [48] which reproduces very well the regime below the micro-cracking onset, $v \leq v_a$ (Fig. 2, thick line). Extrapolation of this regime exhibits [48] a divergence of the dissipated energy for a finite velocity $v'_a = (\alpha - 1)c_R c_D/(\alpha c_D - c_R) \simeq$

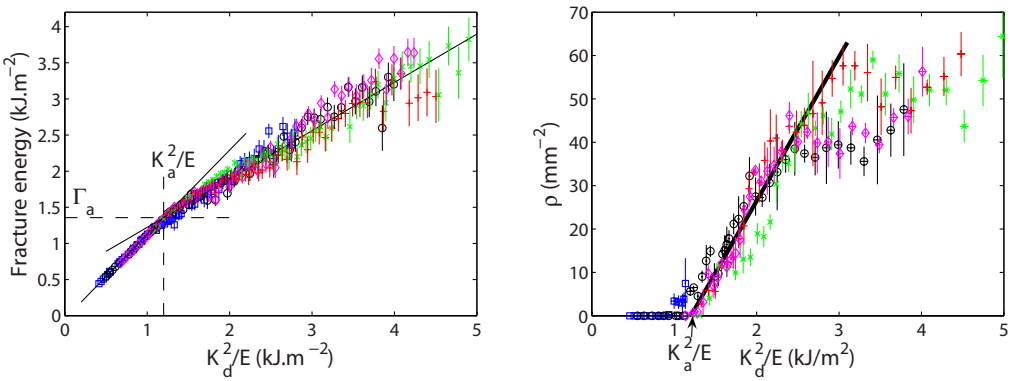

Fig. 5. Adapted from [38]. (a) Dynamic fracture energy Γ as a function of K_d^2/E. A crossover between two linear regimes (linear fits in black lines) occurs at $K_d^2/E = K_a^2/E \simeq 1.2$ kJ.m^{-2}, $\Gamma = \Gamma_a \simeq 1.34$ kJ.m^{-2}). (b) Surface density of conic marks ρ as a function of K_d^2/E (linear fit in black line).

200 m.s^{-1} $\simeq 0.23 c_R$, slightly larger than v_a. In the absence of micro-cracks, this velocity v_a' would have therefore set the limiting macroscopic crack velocity.

For $v \geq v_a$, micro-cracks start to nucleate. The existence of a threshold for micro-cracking appears surprising because it cannot be accounted for by a stress-driven nucleation mechanism only. We believe that the conic marks observed here correspond to the fraction of micro-cracks that have had sufficient time to develop up to optical scale. Indeed, when the FPZ is too small (e.g. for $v \leq v_a$), the nucleated micro-cracks are rapidly caught up by the main crack, only leaving submicrometric elliptic marks, undetectable with ×50 optical microscope.

To interpret the curve $\Gamma(v)$ within the micro-cracking regime, i.e. for $v_a \leq v \leq v_b$, we invoke the existence of an excluded volume V around each micro-crack where stresses are screened and therefore dissipation is prevented. As before, it is interesting to plot the surface density of conic marks $\rho(v)$ as a function of $K_d(v)$ (Fig. 5(b)). Note that the limiting velocity for individual crack/micro-crack tips is expected to be $v_a' \gtrsim v_a$. It is then natural to assume that all micro-cracks propagate at the same velocity v_a in the microcracking regime, which yields $K_d(v) = k(v_a)K$. Between $K_a = K_d(v_a)$ and $K_b = K_d(v_b)$, $\rho(v)$ is observed to scale as:

$$\rho(v) = \beta \frac{K_d(v)^2 - K_a^2}{E} \tag{3}$$

where a fit to the data (R=0.877) gives β =33±3 J^{-1}. This square dependency indicates that the number of conic marks is proportional to the FPZ size and suggests that the density of nucleation sites for micro-cracks is constant within the material. In the micro-cracking regime, the energy $\Gamma(v)S$ dissipated when the crack surface increases by S is $\gamma S + \epsilon(R_c(v)S - \rho(v)S\,V)$, yielding:

$$\Gamma(v) = \Gamma_a + \chi \frac{K_d(v)^2 - K_a^2}{E} \quad \text{with} \quad \chi = \alpha - \epsilon\beta V \tag{4}$$

with Γ_a the fracture energy obtained at $v = v_a$ using Eq. 2. Equation (4) predicts a linear dependence of Γ with $K_d(v)^2/E$, which is in agreement with the measurements for $K_d(v)^2/E > K_a^2/E$ (Fig. 5(a)). A linear fit to the data (R=0,948) gives χ=0.67±0.01.

The corresponding predicted $\Gamma(v)$ [48] reproduces very well the intermediate velocity regime $v_a \leq v \leq v_b$ (Fig. 2) and exhibits a divergence of the dissipated energy for $v_\infty = c_R(1-\chi k(v_a)^2) \simeq 450$ m.s^{-1} $\simeq 0.52 c_R$. This limiting velocity is very close to the observed maximum crack speed in brittle amorphous materials.

5 Conclusion

Both the experimental results and the above discussion shed light on how material defects might control the dynamic fracture of amorphous solids before the onset of micro-branching. For $v < v_a$, the mechanical energy released at the crack tip is dissipated into both a constant surfacic energy and a volumic energy within the FPZ. Since the size of the latter increases rapidly with crack speed, in the absence of micro-cracks, the fracture energy would diverge at a value slightly larger than v_a. At this point, the crack speed would saturate. In reality, through the nucleation, growth and coalescence of micro-cracks, the main crack can reach with a larger effective (macroscopic) velocity [46] [49], up to v_b=0.4c_R. The latter value is determined by the onset of micro-branching, that adds to micro-cracking. We emphasize that the *nominally brittle to quasi-brittle transition* occurring at v_a should be generic for amorphous solids and should therefore be taken into account in future conceptual and mathematical descriptions of dynamic fracture. In particular, a better understanding of the relationship between the dynamics of propagation of both the individual micro-cracks and the macroscopic crack is required.

References

1. A.A. Griffith, Philosophical Transactions of the Royal Society of London, Series A **221**, (1920) 163
2. E. Orowan, Welding Journal, Research Supplement **34** (1955) 157
3. G.R. Irwin, Handbuch der Physik, **6**, (1958) 551.
4. L. Freund, *Dynamic Fracture Mechanics* (Cambridge University Press, Cambridge, England, 1990)
5. H. Bergkvist, Engineering Fracture Mechanics **6**, (1974) 621
6. J. Fineberg and M. Marder, Physics Reports **313**, (1999) 1
7. K. Ravi-Chandar, *Dynamic Fracture* (Elsevier, Amsterdam, The Netherlands, 2004)
8. A. Livne, O. Ben-David and J. Fineberg, Physical Review Letters **98**, (2007) 124301
9. A. Livne, E. Bouchbinder and J. Fineberg, Physical Review Letters **101**, (2008) 264301
10. E. Sharon and J. Fineberg, Nature **397**, (1999) 333
11. J. Fineberg, S.P. Gross, M. Marder and H.L. Swinney, Physical Review Letters **67**, (1991) 457
12. J. Fineberg, S.P. Gross, M. Marder and H.L. Swinney, Physical Review B **45**, (1992) 5146
13. M. Adda-Bedia, M. Ben Amar and Y. Pomeau, Physical Review E **54**, (1996) 5774
14. P. Gumbsch, S.J. Zhou, B.L. Holian, Physical Review B **55**, (1997) 3445
15. M. Adda-Bedia, R. Adias, M. Ben Amar and F. Lund, Physical Review Letters **82**, (1999) 2314
16. M. Adda-Bedia, Physical Review Letters **93**, (2004) 185502
17. H. Henry and H. Levine, Physical Review Letters **93**, (2004) 105504
18. E. Bouchbinder, J. Mathiesen and I. Procaccia, Physical Review E **71**, (2005) 056118
19. R. Spatschek, M. Hartmann, E. Brener, H. Muller-Krumbhaar and K. Kassner, Physical Review Letters **96**, (2006) 015502
20. D. Pilipenko, R. Spatschek, E.A. Brener and H. Muller-Krumbhaar, Physical Review Letters **98**, (2007) 015503
21. E. Katzav, M. Abba-Bedia and A. Arias, International Journal of Fracture, **143**, (2007) 245
22. H. Henry, EPL **83**, (2008) 16004
23. J.F. Kalthoff, S. Winkler and J. Beinert, International Journal of Fracture **71**, (1976) 317
24. A.J. Rosakis, J. Duffy and L.B. Freund, Journal of the Mechanics and Physics of Solids **32**, (1984) 443
25. C. Fond and R. Schirrer, Comptes Rendus de l'Académie des Sciences de Paris *329*, (2001) 195
26. A. Bertram and J.F. Kalthoff, Materialprüfung **45**, (2003) 100
27. D. Hull, *Fractography: Observing, Measuring and Interpreting Fracture Surface Topography* (Cambridge University Press, Cambridge, England,
28. J.W.Johnson and D.G. Holloway, Philosophical Magazine **14**, (1966) 731
29. J.F. Boudet, S. Ciliberto and V. Steinberg, Europhysics Letters **30**, (1995) 337
30. T. Cramer, A. Wanner and P. Gumbsch, Physical Review Letters **85**, (2000) 788
31. D. Bonamy and K. Ravi-Chandar, Physical Review Letters **91**, (2003) 235502
32. D. Bonamy and K. Ravi-Chandar, International Journal of Fracture **134**, (2005) 1

33. G. Wang, Y.T. Wang, Y.H. Liu, M.X. Pan, D.Q. Zhao and W.H. Wang, Applied Physics Letters **89**, (2006) 121909
34. M.J. Buehler and H. Gao, Nature **439**, (2006) 307
35. G. Wang, D.Q. Zhao, H.Y. Bai, M.X. Pan, A.L. Xia, B.S. Han, X.K. Xi, Y. Wu and W.H. Wang, Physical Review Letters **98**, (2007) 235501
36. A. Rabinovitch and D. Bahat, Physical Review E **78**, (2008) 067102
37. B. Lawn, *Fracture of Brittle Solids* (Cambridge University Press, Cambridge, England, 1993)
38. J. Scheibert, C. Guerra, F. Célarié, D. Dalmas and D. Bonamy, Physical Review Letters **104**, (2010) 045501
39. E. Bruhwiler and F.H. Wittmann, Engineering Fracture Mechanics **35**, (1990) 117
40. B.L. Karihaloo and Q.Z. Xiao, International Journal of Fracture **112**, (2001) 120
41. V. R.Regel, Zhurnal Tekhnicheskoi Fiziki **21**, (1951) 287
42. A. Smekal, Osterreich Ingenieur Archiv **7**, (1953) 49
43. J. A. Kies and G. R. Irwin, Journal of Applied Physics **21**, (1950) 716
44. G. R. Irwin and J. A. Kies, Welding Journal Research Supplement **31**, (1952) 95
45. K. Ravi-Chandar and W.G. Knauss, International Journal of Fracture **26**, (1984) 141
46. K. Ravi-Chandar and B. Yang, Journal of the Mechanics and Physics of Solids **45**, (1997) 535
47. D.E.Moore and D.A. Lockner, Journal of Structural Geology **17**, (1995) 95
48. C. Guerra *et al*., to be published
49. S. Prades, D. Bonamy, D. Dalmas, E. Bouchaud and C. Guillot, International Journal of Solids and Structures **42**, (2005) 637